Modelling of Metal Oxide Surge Arresters in Simulation Software DYNAST

Vladislav Síťař [1] and Jan Veleba [2]

[1] Jan Evangelista Purkyně University, Department of Energy and Electrical Engineering, Ústi nad Labem, Czech Republic, e-mail: *sitar@fvtm.ujep.cz*

[2] ABB s.r.o., Operation Center Czech Republic, Process Automation Division, Ostrava, Czech Republic, e-mail: *jan.veleba@cz.abb.com*

Abstract — **This paper describes the possibilities for mathematical modelling of gap-less surge arresters in the simulation software DYNAST. This tool does not belong to standard modelling softwares in the field of electric power engineering. However, it may provide some key advantages when compared to more frequently used software such as EMTP-ATP and MATLAB-Simulink. Description of the metal oxide varistor modelling at temporary and switching overvoltages, fast-front states, and lightning strokes is presented. More information about the defined internal structure of the surge arrester models and ways for implementing respective V-I characteristics are provided. To verify the correct behaviour of the models, both slow and fast overvoltage scenarios are simulated and evaluated.**

Keywords — metal oxide varistor (MOV), gap-less surge arrester, surge arrester model, V-I characteristic of the surge arrester, temporary and switching overvoltages, lightning stroke, simulation software DYNAST

I. Introduction

Surge arresters have been used in electrical networks for electrical protection against overvoltages. They eliminate unfavourable effects of an overvoltage state on the insulation of individual network elements and equipment. Gap-less surge arresters, consisting of one or more nonlinear voltage-dependent varistors of zinc oxide, have been used in both transmission and distribution systems for decades.

The target of the surge arrester modelling is to find out, what voltages occur in the arrester connection point (called residual voltage) when an overvoltage wave is passing through it (analysing the residual voltage magnitude). Overvoltage waves have negative effect on the equipment insulation and hence, they must be accurately quantified.

The non-linear voltage dependent varistors have been mathematically modelled by controlled current sources in standard simulation softwares [1]. They supply the current into the network depending on the voltage in the arrester connection point in accordance with the defined V-I characteristic. Using this model, it is possible to simulate the arrester behaviour under temporary or slow-front switching overvoltages.

For fast-front overvoltage states, such as lightning strokes or switching waves with high steepness of wave front, the current-based MOV model becomes highly unreliable. This is caused mainly by the dependence of the zinc oxide varistor elements on frequency. Voltage in the arrester connection point is the function of both steepness and amplitude of the overvoltage wave. Therefore, other parameters must be considered as well to include the effect of boundary conditions and thus, to represent the behaviour of the varistor correctly. The parameters, which significantly affect the behaviour of the surge arrester at fast frequency overvoltage states, are mainly: the inductances of the varistor elements and of conductors for connecting the surge arrester to the network and to the ground [2].

Up to now, several gap-less varistor surge arrester models have been created. The most-known model is the IEEE model, also called the Frequency-dependent model [2]. This model is composed of two nonlinear voltage-dependent varistors (A0, A1) with the respective V-I characteristics implemented, the capacitor (C) representing the capacitance of the surge arrester, and two frequency filters (R0-L0, R1-L1), which separate the varistors from the network and from each other (see Fig. 1). The last mentioned frequency filters have also the most significant impact on the shape of fast-front overvoltage waves. All parameters of the model above can be calculated from construction and other catalogue data of the arrester manufacturer.

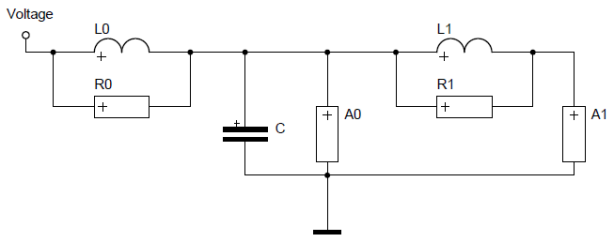

Fig. 1. The IEEE model [2].

The majority of other competitive models have been derived from the IEEE model. They have a similar internal structure and parameters computed when considering other assumptions as well. The well-known examples are the Pinceti-Giannettoni model [3] (Fig. 2) and Fernández-Díaz model [4] (Fig. 3). Although the Conventional model [5] (Fig. 4) belongs to less sophisticated models, it is frequently used as well. The Mardir-Saha model [6] is also derived from the IEEE model, but with a modified internal structure. On the other hand, original models such as the Tominaga model [7], Kim model [8], Popov model [9] or others seem also promising for various applications. Individual models, internal structures, and their comparison in simulations of the lightning strokes in EMTP/ATP are further presented

TELEN2016017
DOI 10.14311/TEE.2017.1.021

by the authors in [5], [10]–[15]. The results are different in terms of the arrester voltage waveform at the current wave propagation. The differences are especially in the residual voltage magnitude (and time instant) at the current impulse peak value, voltage steepness of front and tail impulse section, and their durations. The accuracy of each model depends mainly on the amount of internal elements and methodology of their calculation. The accuracy can be evaluated when comparing the voltage and current waveforms of each model to the measured or expected data. According to the authors in [11], the most accurate models are both Pinceti-Giannettoni and Fernández-Díaz models, which have constant parameters computed by using the authors' equations and relevant manufacturer data. It can be concluded that all models mentioned above are more suitable for fast-front impulses.

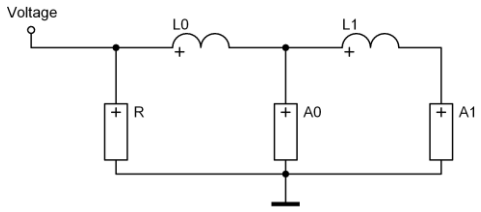

Fig. 2. The Pinceti-Giannettoni model [3].

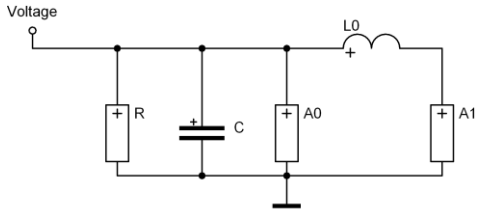

Fig. 3. The Fernández-Díaz model [4].

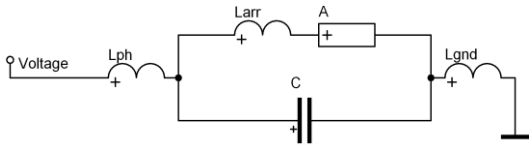

Fig. 4. The Conventional model [5].

II. Modelling of Temporary and Switching Overvoltages

Temporary overvoltages can be modelled by higher amplitudes of the supply voltage when above a specific limit. The switching overvoltages are often simulated using switching waves or impulses, which last for tens to hundreds of microseconds or even several milliseconds for the front section and tens of milliseconds for the halve-tail section. It is possible to use the normalised switching impulse of 250/2500 μs [16] with a variable amplitude.

III. Modelling of Lightning Strokes

High-frequency waves, such as lightning strokes and fast-front transients, are usually modelled by current waves, which are generated by the current source with a negative polarity. The surge parameters are: front time, wave amplitude, and decline time. Current waves have usually time parameters of 8/20 μs (front/half-tail) with variable amplitudes from 10 to 40 kA for HV [17] and 2.5, 5, 10 or 20 kA for MV [18]. There are other normalized current waves as well, which have been used for testing of the surge arresters on lightning strokes, e.g. 1/2 μs with variable amplitudes. The authors in [5], [10]–[12] used test waves above for simulations of individual arrester models.

Note: In accordance with [19], [20], immunity tests are required for equipment use in residential, commercial, light-industrial, and industrial environments. The surges are defined as line-to-earth and line-to-line with 1.2/50 (8/20) μs. For fast transients, the waves are normalized with 5/50 ns and repetition frequency of 5 or 100 kHz (commonly used).

IV. Input Data for Surge Arrester Modelling

The input data are usually provided by manufacturer catalogues of compact surge arresters and its elements. The varistor V-I characteristic, nominal and maximum discharge current at 8/20 μs, and the surge current (or residual voltage) are of the highest importance. The construction parameters of the entire surge arrester, i.e. the number of varistor elements, the number of their parallel sections, and wire lengths to the line and to the ground are needed as well.

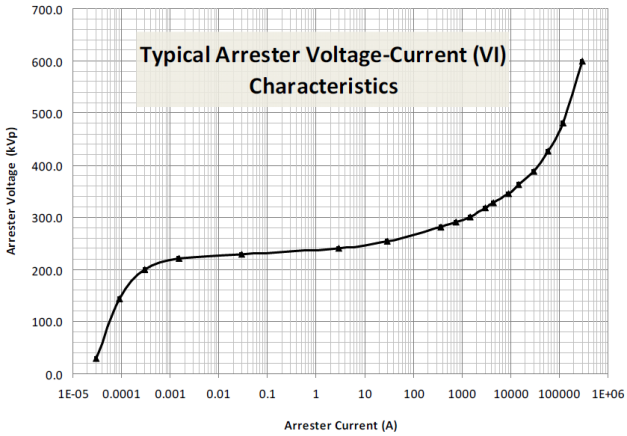

Fig. 5. Typical V-I characteristic of the MOV [21].

A typical arrester V-I characteristic is presented in [21], see Fig. 5. The characteristic consists of three parts, which describe the arrester behaviour under a) nominal operating state (approx. up to 1 mA), b) weak overvoltage state with small voltage increase above the maximum operating voltage (roughly linear part of the V-I characteristic), and c) strong overvoltage state with high voltage magnitudes corresponding to lightning strokes (high current and voltage steepness). All these parts can be described by using exponential equation (1), see in [10], [11]. However, a more suitable formula for the mathematical modelling is presented in [22], see (2).

$$i = p\left(\frac{v}{V_{ref}}\right)^{q} \tag{1}$$

TELEN2016017
DOI 10.14311/TEE.2017.1.021

$$\frac{v}{V_{ref}} = k\left(\frac{i}{I_{ref}}\right)^{1/\alpha} \quad (2)$$

The parameters v and i are the actual voltage and current flowing through the arrester, respectively. The coefficients k, p, q, and α are the constants related to the relevant parts of the arrester V-I characteristic. The I_{ref} is the current flowing through one element of the MOV when the voltage on the arrester is equal to the reference voltage V_{ref}. Both I_{ref} and V_{ref} are usually provided in manufacturer datasheets.

V. Simulation Software DYNAST

The simulation software DYNAST has been used for a highly robust computer modelling of dynamic systems. It contains models from various technical fields in its libraries, e.g. for heat transfer, mechanics, electronics, electro-mechanics, and others. Additionally, it provides a fundamental modelling by means of block schemes [23]. For the field of electric power engineering, however, the relevant libraries are not comprehensively covered by an appropriate element or equipment models.

DYNAST offers many advantages for its users – see those most important below. Conversion and transfer of DYNAST models into MATLAB-Simulink [22] is one of its beneficial features as well [23], [24].

Advantages of DYNAST [25], [26]:

- the possibility of modelling problems from various technical disciplines,
- high computational efficiency in comparison to other softwares when solving nonlinear tasks,
- various model formulations are possible. The model can be defined by i) combination of differential equations, ii) block schemes (as in MATLAB-Simulink), iii) physical relations schemes, which characterize physical properties of individual elements or complex systems; or iv) their combination,
- the possibility of creating own library elements and special models for solving specific tasks.

For the transient analyses, DYNAST uses the implicit multistep integration method with the backward differentiation formula. The integration step size and method order are both continuously optimized by DYNAST during the integration process with respect to the actual shape of the resulting response [24].

VI. Surge Arrester Model in DYNAST

All models (see Figs. 1 to 4) were used by the authors for simulation purposes. A combination of physical schemes with the systems of equations appears as the most appropriate in DYNAST. The physical schemes correspond to internal structures of the referenced arrester models.

The relevant V-I characteristics are assigned to the individual varistors in the model. They may be defined in two ways: i) by individual points, which can be obtained from catalogues or measurements (see Fig. 5); or ii) by three exponential functions with their effects limited by logical conditions, i.e. by specific arrester currents flowing through the arrester at specific voltages. Note: By approach ii), the arrester V-I characteristic is also defined e.g. in MATLAB-Simulink.

In fact, approach ii) is more appropriate due to better smoothness of the resultant waveforms. This is automatically accomplished by DYNAST, which applies the linear interpolation method between individual points. The values of coefficients k and α can be determined by using the equations in [27] or by the mathematical deduction.

A. Testing of Temporary Overvoltages

For temporary overvoltages and low-front switching waves, the arrester model consists only of the current source with the implemented V-I characteristic. The model behaviour is verified on a simple circuit (Fig. 6). The temporary overvoltage (i.e. variable amplitude above the maximum operating AC voltage) or superposed wave (250/2500 μs waves with a variable amplitude) must be adjusted to the voltage level of the arrester. In this case, the amount of accumulated energy or thermal stress does not need to be considered [28]. However, more sophisticated models must take these issues into account due to a possible thermal or physical damage at high temperatures of the varistor or when huge amount of energy is to be absorbed.

Circuit parameters

Source	750 V, 50 Hz
Stabilizing resistance R1	1 Ω
Line1	0.2 Ω, 1 mH, 10 nF
Line2	0.2 Ω, 1 mH, 10 nF
Load1	2 kW, PF 0.95
Load2	2 kW, PF 0.95

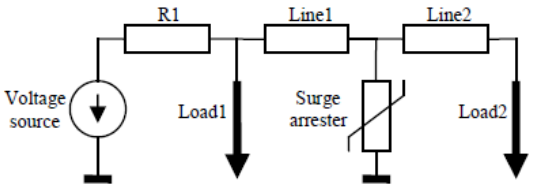

Fig. 6. Single line diagram for arrester model verification (temporary and switching overvoltages).

In simulations, the LV metalized square disc varistor [29] with an adapted V-I characteristic is used (see Fig. 7). The red solid lines limit the sections introduced in Chapter IV., i.e. the normal operating state section (a), the weak overvoltage state section (b), and the strong overvoltage state section (c). The latter is divided by the red dashed line due to a better mathematical description of the V-I characteristic by using Eq. 2 (see Tab. I.). In this case, the limit voltage is approximate 790 V_p.

TABLE I.
Parameters of the V-I Characteristic

Voltage interval		Parameters
		V_{ref} = 430 V, I_{ref} = 1 mA
a)	230 – 430	k = 0.9994, α = 7.36
b)	430 – 600	k = 1, α = 25.565
c)	600 – 790	k = 0.897, α = 19.275
	790 – 1 000	k = 0.749, α = 15.402

TELEN2016017
DOI 10.14311/TEE.2017.1.021

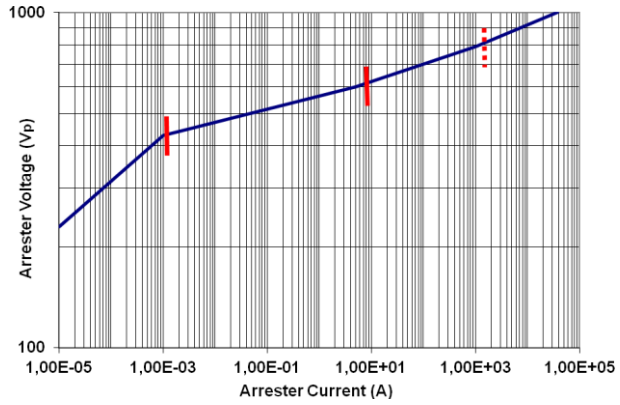

Fig. 7. Adapted V-I characteristic of the MOV.

The results are relatively reliable since the arrester current corresponds to the defined voltage points in the V-I characteristic. Two periods of the arrester voltage and current waveforms at a temporary overvoltage are shown in Fig. 8. The overvoltage value is chosen as the double of the nominal voltage amplitude (i.e. 650 V_P). Both reduction of the voltage amplitude and current rise are evident when the voltage in the connection point reaches the respective value. The higher overvoltage occurs the more significant voltage reduction arises.

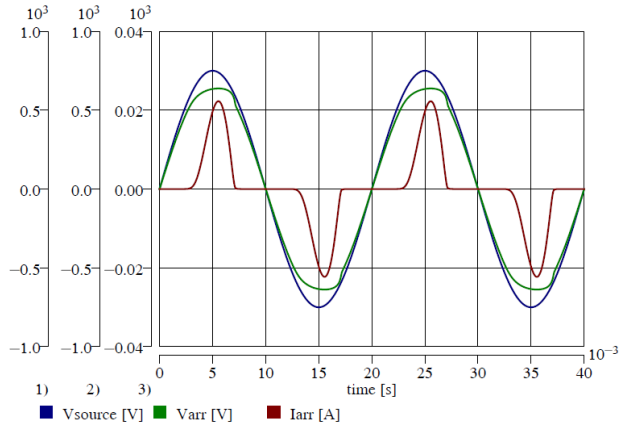

Fig. 8. Voltage and current waveforms in the arrester connection point (temporary overvoltage study case).

B. Testing of Switching Overvoltages

The voltage and current waveforms at the switching overvoltage are shown in Fig. 9. The voltage pulses of 250/2500 μs have the 650 V amplitude superposed to the front voltage section (1st voltage period) and the 650 V amplitude superposed to the zero voltage time (2nd voltage period). It is visible that the voltage is reduced when the voltage level is reached. Additional simulations in MATLAB-Simulink, EMTP/ATP, and DYNAST were carried out and the results compared in [30], [31].

C. Testing of Lightning Overvoltages

For atmospheric overvoltages, the model is composed of two varistors and passive elements (similarly as in Fig. 1). The source, which generates the current waves with negative polarity, is connected to them. The single line diagram does not contain any line or load elements, but only the current impulse source and the arrester. The methodology, which is introduced in [2], is used to calculate the points of the V-I characteristic. The points up to 0.01 kA (for A0) and 0.1 kA (for A1) are adapted by the authors, although any referenced source does not use such small currents in the methodology. The remaining passive parameters are calculated by using the methodology for the Pinceti-Giannettoni model [3] and the Fernández-Díaz model [4]. The manufacturer catalogue [27] and measurement data are used as the input for creating the V-I characteristic (see Fig. 10). For both characteristics A0 and A1, the section with leakage currents of up to 0.1 A is derived from the V-I characteristic introduced in [17]. The V-I points between the leakage part and the part described in the methodology (i.e. from 0.1 A to 10 A for A0 and from 0.1 A to 100 A for A1) are suitably chosen when respecting the smoothness and growing trend of the characteristic. The error of this curve adaptation does not have significant impact on the solution accuracy, since the simulation results do not belong to this area, but to the voltage peak area. If the error is too high, however, it may negatively affect numerical stability of the applied mathematical methods.

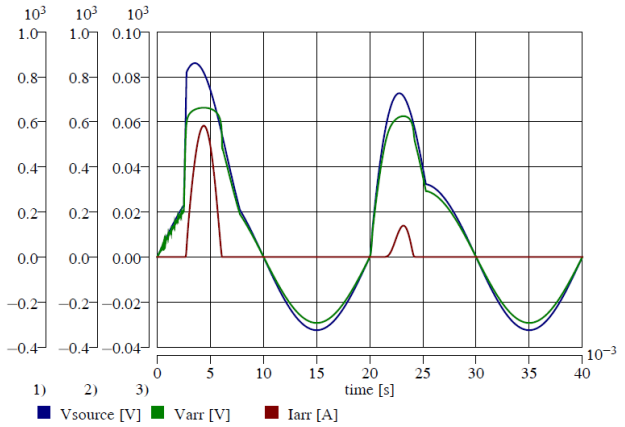

Fig. 9. Voltage and current waveforms in the arrester connection point (superposed switching wave study case).

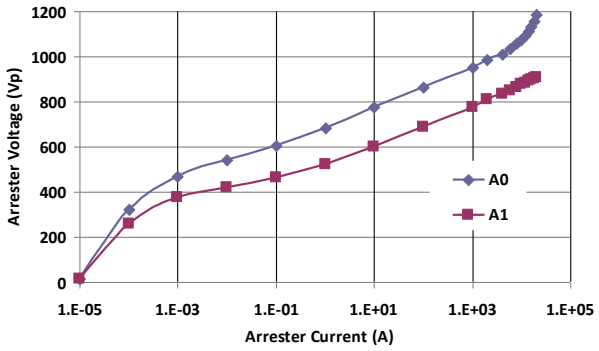

Fig. 10. Adapted V-I characteristics for fast-front waves.

For simulation purposes, a typical discharge current wave of 8/20 μs was created with different amplitudes. DYNAST does not contain the generator of the current or voltage pulses. It is possible to create a current pulse by using the pulse function, but it is not suitable because of

TELEN2016017
DOI 10.14311/TEE.2017.1.021

insufficient smoothness of the resulting waveform. Hence, the waveform points were deducted from the measurement data.

For the 20 kA wave and the IEEE model applied, the voltage and current waveforms are shown in Fig. 11. In this case, the residual voltage at the current amplitude is 908 Vp. This value does not correspond to the manufacturer or measured data (1,049 Vp). This discrepancy is also visible for other residual voltages. It was further observed that the simulated residual voltages were always smaller than those obtained from manufacturer catalogues or measurements. This can be caused by the input data or used methodology. The manufacturer declares only a typical V-I characteristic for a given varistor, which can be slightly different because of a tolerance range. Number of the test impulses and varistor temperature can significantly influence the results. When compared to a given V-I characteristic, the data variance can reach ± 10 % for the same test impulse. The calculation methodology for the A0 and A1 varistors and for passive elements is derived from the EHV arresters. The varistor capacitance, for example, is 3.5 nF based on manufacturer data, but 23.3 nF after the calculation in [2]. Other parameters cannot be compared, as the manufacturers do not provide them. The voltage waveform is also influenced by the shape and smoothness of the current wave, which is not ideal.

In comparison to results in [11], the waveforms are not identical with respect to time. For example, the highest arrester voltage is not reached before the current amplitude. The model dynamic behaviour is also missing. The results are more similar to those of the Conventional model in [11].

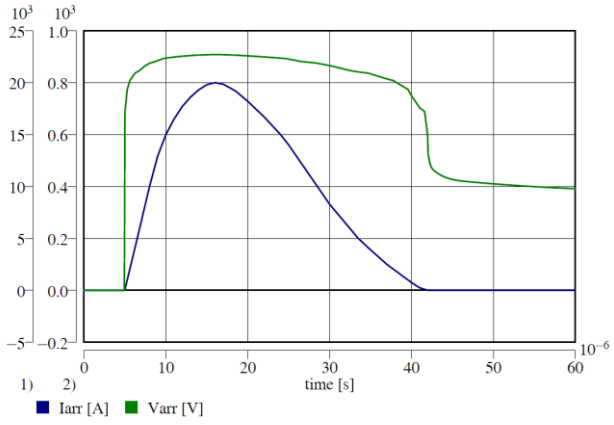

Fig. 11. Voltage and current on the varistor (8/20 μs, 20 kA wave; the IEEE model).

The parameters of the Pinceti-Giannettoni model are calculated identically as for the IEEE model. However, the values of the passive parameters are slightly different. The arrester voltage and current waveforms for 8/20 μs, 20 kA wave are shown in Fig. 12. The voltage waveform corresponds to results of the IEEE model in both front and peak sections of the wave, but not in the tail section, where the voltage falls faster. This is caused by the magnitudes of the model passive parameters, especially of the nonlinear resistors. The calculated residual voltage does not correspond to the V-I characteristic from the catalogue or measurements. In both of these cases, the residual voltage amplitudes are smaller by approximate 141 Vp. Similar results are achieved also with other amplitudes of the current waves.

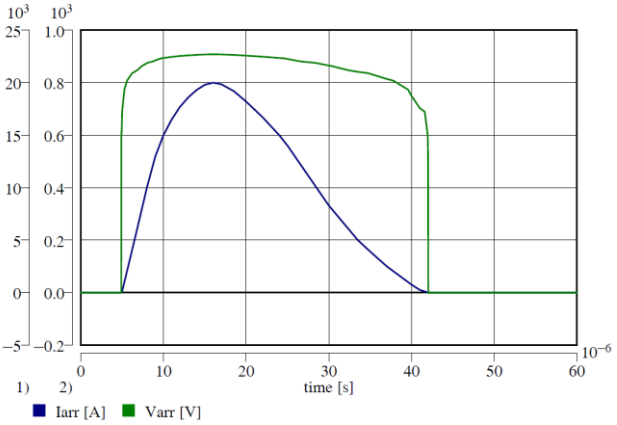

Fig. 12. Voltage and current on the varistor (8/20 μs, 20 kA wave; the Pinceti-Giannettoni model).

For the Fernández-Díaz model, the calculation of the passive parameters differs from both formerly described models. In this model, the current flowing through each varistor is calculated based on the varistors constant current ratio. The resultant voltage and current waveforms for 8/20 μs, 20 kA wave are shown in Fig. 13. The varistor voltage has a similar waveform as in both previous models. However, its residual voltage corresponds to the V-I characteristic of the varistor A1. The varistor A0 has almost no effect. The voltage and current amplitudes are reached in the same time. Also, the results are relatively good in comparison to the measured data. The residual voltage is 1,049 Vp (measured) and 1,130 Vp (simulated, see Fig. 13). The most significant difference is in the varistor voltage at current extinction (impulse tail). This part is mainly influenced by the varistor capacitance. When using the capacitance value from the catalogue, however, the voltage gets closer to the measured data.

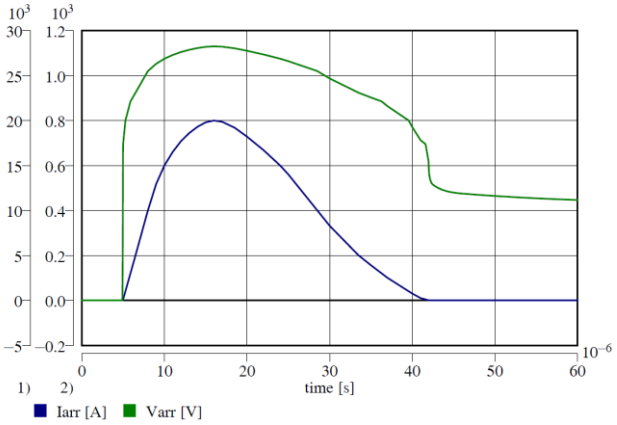

Fig. 13. Voltage and current on the varistor (8/20 μs, 20 kA wave; the Fernández-Díaz model).

Internal structure of the Conventional model consists of only one nonlinear resistor with the implemented V-I characteristic from the manufacturer catalogue. As introduced in [5], the methodology is used for the calculation of inductances, which connect the arrester to the phase and to the ground. Since the author in [5]

TELEN2016017
DOI 10.14311/TEE.2017.1.021

introduces the inductance calculation for the circular varistors only, the internal inductance of the rectangular varistor is derived and calculated by the equation in [32]. Arrester capacitance is not computed, as it is given by the catalogue.

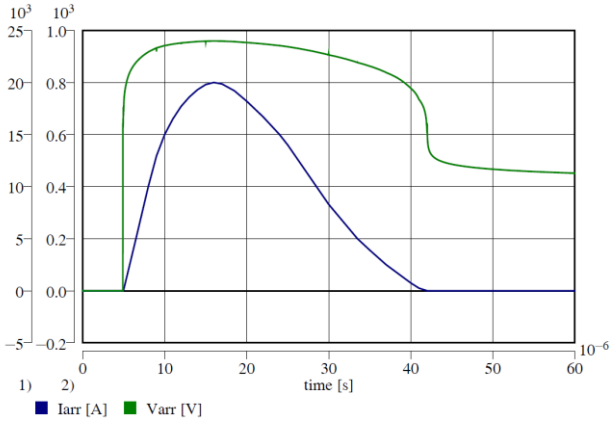

Fig. 14. Voltage and current on the varistor (8/20 µs, 20 kA wave; the Conventional model).

Simulation results of the Conventional model are satisfying (Fig. 14). The residual voltage amplitude reaches 960 V_P, which is only 89 V_P below the measured value. Magnitudes of the passive parameters have no influence on the residual voltage. However, the Conventional model is very sensitive about the smoothness of the current wave. For avoiding significant voltage oscillations, the current impulse was defined by a larger amount of points. The residual voltage reaches the peak at the current amplitude. This corresponds to both measured data and model behaviour described in [5]. When compared to the measured data, the error in the front section is not visible. This is caused by the magnitudes of the passive parameters, especially of inductances, which are smaller than those in the Fernández-Díaz model, for example.

The voltage and current waveforms of the SIOV-D40K275 varistor for 8/20 µs, 20 kA wave obtained by measurement are presented in Fig. 15. The voltage waveform contains superposed oscillations, which are caused by the interaction of the surge voltage generator, varistor, and connected conductors. The results are very similar to those of the Conventional model.

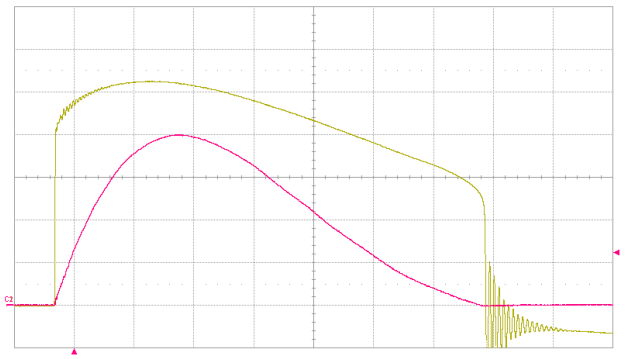

Fig. 15. Voltage and current on the varistor (8/20 µs, 20 kA wave; SIOV-D40K275 varistor (200 V/div, 5 kA/div)).

VII. Conclusion

It is possible to model and verify correct behaviour of a gap-less surge arrester in DYNAST. DYNAST calculation methods work reliably on nonlinear tasks, the modelled system does not collapse, and the results do not diverge. By using the libraries of physical elements, the user can create the arrester models with the behaviour corresponding to the reality at temporary and switching overvoltages. It was further verified that the simulation results (residual voltages) correspond to the catalogue data.

The simulations of the fast-front surges and lightning strokes can be also performed in DYNAST. However, the outputs should be used only for guidance. Methodologies for the calculation of parameters in each arrester model were originally derived by their authors for the HV and EHV arresters. As shown in this paper, however, they can be suitably utilized for the LV arresters as well. The simulation results are not in exact compliance with theoretical assumptions of the residual voltage amplitude and time synchronism of the current wave peak and residual voltage amplitude as provided by the IEEE and Pinceti-Giannettoni models. For the modelling purposes, the manufacturer catalogue data or measurement data must be used as the input to the arrester models. The Conventional model appears to be the most reliable from all simulated models. Its voltage peak and waveform outputs are very similar to the measured and expected data. The difference between the measured and simulated voltage peak value is only 89 V_P. This value corresponds to expected variance of the measurement data.

Acknowledgment

I would like to thank to Mr. Milan Duda and to his colleagues from company SALTEK, Usti nad Labem for providing relevant product data and other outputs from measurements performed in the company laboratory.

References

[1] H. Mann, *Využití počítače při elektrotechnických návrzích*, 1st ed., Praha: SNTL, 1984.

[2] IEEE Working Group 3.4.11, "Modeling of metal oxide surge arrester," *IEEE Transaction on Power Delivery*, vol. 7, no. 1, Jan. 1992, pp. 302-309. [Online]. Available on: DOI: 10.1109/61.108922 [Accessed: 3rd Nov. 2015]. https://doi.org/10.1109/61.108922

[3] P. Pinceti and M. Giannettoni, "A simplified model for zinc oxide surge arrester," *IEEE Transaction on Power Delivery*, vol. 14, no. 2, Apr. 1999, pp. 393-398. [Online]. Available on: DOI: 10.1109/61.754079 [Accessed: 3rd Nov. 2015]. https://doi.org/10.1109/61.754079

[4] F. Fernández and R. Díaz, "Metal-oxide surge arrester model for fast transient simulations," In *Proceedings of the International Conference on Power Systems Transients (IPST)*, Rio de Janeiro, 2001, pp. 1-6. [Online]. Available on: http://www.ipstconf.org/papers/Proc_IPST2001/01IPST056.pdf [Accessed: 3rd Nov. 2015].

[5] P.M. Miguel, "Comparison of Surge Arrester Models," *IEEE Transaction on Power Delivery*, vol. 29, no. 1, Sep. 2013, pp. 21-28. [Online]. Available on: DOI: 10.1109/TPWRD.2013.2279835 [Accessed: 3rd Nov. 2015]. https://doi.org/10.1109/TPWRD.2013.2279835

[6] K.P. Mardira and T.K. Saha, "A simplified lightning model for metal oxide surge arrester," The University of Queensland – Australia, 2011. [Online]. Available on: https://espace.library.uq.edu.au/view/UQ:9806/A_Simplified_Lig.pdf [Accessed: 4th Nov. 2015].

[7] S. Tominaga, K. Azumi, Y. Shibuya, M. Imataki, Y. Fujiwara, and S. Nishida, "Protective Performance of Metal Oxide Surge Arrester Based on the Dynamic V-I characteristics," *IEEE Transaction on Power Apparatus and Systems*, vol. PAS-98, no. 6, 1979, pp. 1860-1871. [Online]. Available on: DOI: 10.1109/TPAS.1979.319359 [Accessed: 6th Jan. 2016].
https://doi.org/10.1109/TPAS.1979.319359

[8] I. Kim, T. Funabashi, H. Sasaki, T. Hagiwara, and M. Kobayashi, "Study of ZnO arrester model for steep front wave," *IEEE Transactions on Power Delivery*, vol. 11, no. 2, 1996, pp. 834-841. [Online]. Available on: DOI: 10.1109/61.489341 [Accessed: 6th Jan. 2016]. https://doi.org/10.1109/61.489341

[9] M. Popov, L. van der Sluis, and G.C. Paap, "Application of a New Surge Arrester Model in Protection Studies Concerning Switching Surges," *IEEE Power Engineering Review*, vol. 22, no. 9, 2002, pp. 52-53. [Online]. Available on [Accessed: 6th Jan. 2016]:
https://doi.org/10.1109/MPER.2002.4312562

[10] A. Bayadi, N. Harid, K. Zehar, and S. Belkhait, "Simulation of metal oxide surge arrester dynamic behavior under fast transients," In *Proceedings of the International Conference on Power Systems Transients (IPST)*, New Orleans, 2003, pp. 1-6. [Online]. Available on: http://ipstconf.org/papers/Proc_IPST2003/03IPST14b-01.pdf [Accessed: 3rd Nov. 2015].

[11] A. Meister, R.A. Shayany, and M.A.G. Oliveira, "Comparison of metal oxide surge arrester models in overvoltage studies," *International Journal of Engineering, Science and Technology*, vol. 3, no. 11, 2011, pp. 35-45. [Online]. Available on [Accessed: 3rd Nov. 2015]: https://doi.org/10.4314/ijest.v3i11.4S

[12] D. Lovrič, S. Vujevič, and T. Modrič, "Comparison of Different Metal Oxide Surge Arrester Models," *International Journal of Emerging Science*, vol. 1, no. 4, Dec. 2011, pp. 545-554. [Online]. Available on: http://journaldatabase.info/articles/comparison_different_metal_oxide_surge.html [Accessed: 3rd Nov. 2015].

[13] S.A. Ali, "Design of Lightning Arresters for Electrical Power Systems Protection," *Advances in Electrical and Electronic Engineering (AEEE)*, vol. 11, no. 6, Dec. 2013, pp. 433-432. [Online]. Available on [Accessed: 3rd Nov. 2015]:
https://doi.org/10.15598/aeee.v11i6.661

[14] C.A. Christodoulou, F.A. Assimakopoulou, I.F. Gonos, and I.A. Stathopulos, "Simulation of Metal Oxide Surge Arresters Behavior," *IEEE Power Electronics Specialists Conference (PESC)*, June 2008, pp. 1862-1866. [Online]. Available on [Accessed: 3rd Nov. 2015]:
https://doi.org/10.1109/PESC.2008.4592215

[15] S. Dau, "Modelling of metal oxide surge arresters as elements of overvoltage protection systems," *International Conference on Lightning Protection (ICLP)*, Vienna, Sep. 2012, pp. 1-5. [Online]. Available on [Accessed: 6th Nov. 2015]:
https://doi.org/10.1109/ICLP.2012.6344236

[16] ČSN EN 60060-1. Technika zkoušek vysokým napětím – Část 1: Obecné definice a požadavky na zkoušky.

[17] IEC 60099-4:2014, ed. 3.0. Surge arresters – Part 4: Metal-oxide surge arresters without gaps for a.c. systems.

[18] IEEE TF on Fast Front Transients, "Modeling guidelines for fast transients," *IEEE Transaction on Power Delivery*, vol. 11, no. 1, Jan. 1996, pp. 493-506. [Online]. Available on: DOI: 10.1109/61.484134 [Accessed: 3rd Nov. 2015].

[19] IEC 61000-6-1:2016, ed. 3.0. Electromagnetic compatibility (EMC) - Part 6-1: Generic standards - Immunity standard for residential, commercial and light-industrial environments.

[20] IEC 61000-6-2:2016, ed. 3.0. Electromagnetic compatibility (EMC) - Part 6-2: Generic standards - Immunity standard for industrial environments.

[21] K. Patil and C. Grande-Moran, "Modeling Metal Oxide Varistors (MOV) in Short Circuit Calculations," SIEMENS – Power Technology, no. 111, March 2012, pp. 1-6. [Online]. Available on: http://w3.usa.siemens.com [Accessed: 6th Nov. 2015].

[22] Homepage of MATLAB-Simulink. [Online]. Available on: http://www.mathworks.com [Accessed: 6th Nov. 2015].

[23] H. Mann and M. Ševčenko, *Snadné počítačové modelování dynamických soustav*. Praha: ČVUT, 2008.

[24] Homepage of DYNAST. [Online]. Available on: http://virtual.cvut.cz/dynastcz/ [Accessed: 2nd Nov. 2015].

[25] L. Noháčová and K. Noháč, "Nové modely pro elektroenergetiku simulačního nástroje DYNAST," In *Proceedings of the 13th International Scientific Conference Electric Power Engineering (EPE)*, pp. 201–204, Brno 2012.

[26] L. Noháčová and K. Noháč, "Nové možnosti přístupu k modelování v elektroenergetice," In *Proceedings of the 10th International Scientific Conference Electric Power Engineering (EPE)*, pp. 1–3, Ostrava 2009.

[27] J. Woodworth, "Understanding Arrester Discharge Voltage," ArresterWorks - ArresterFacts 013, Dec. 2008, pp. 1-8. [Online]. Available on: http://www.arresterworks.com [Accessed: 6th Nov. 2015].

[28] J. Woodworth, "Understanding the Arrester Energy Handling Issue," ArresterWorks - ArresterFacts 012, Nov. 2008, pp. 1-6. [Online]. Available on: http://www.arresterworks.com [Accessed: 6th Jan. 2016].

[29] Metal Oxide Varistors – Metallized square disc, SIOV-D40K275Q, EPCOS. Internal documentation of SALTEK Company.

[30] V. Síťař, K. Noháč, U. Schmidt, and J. Veleba, "Modeling of surge arresters during temporary overvoltage conditions in alternative simulation tools," In *Proceedings of the 5th International Scientific Conference Control of Power Systems*, pp. 1-6, Tatranské Matliare 2014.

[31] V. Síťař, *Tvorba modelovacích analytických nástrojů v oboru elektroenergetiky s důrazem na oblast spolehlivosti a provozu venkovních vedení*, Dissertation, University of West Bohemia, pp. 61-77, Pilsen, 2016.

[32] Z. Piatek, B. Baron, T. Szczegielniak, D. Kusiak, and A. Pasierbek, "Self inductance of long conductor of rectangular cross section," *Przeglad Elektrotechniczny*, vol. 8, no. 88, 2012, pp. 323-326. [Online]. Available on: http://www.red.pe.org.pl [Accessed: 7th Jan. 2016].

TELEN2016017
DOI 10.14311/TEE.2017.1.021